Influence of powder mixing method on properties of high entropy alloys of FeCrMnAlMo thin coatings obtained by magnetron sputtering

Y.Y. Santana, Mourtada-Aly Sow, Corinne Nouvellon, Catherine Cordier, Franck Béclin, Matthieu Touzin, A. Tromont, Xavier Noirfalise, Laurent Boilet, Jean-François Trelcat, et al.

Influence of powder mixing method on properties of high entropy alloys of FeCrMnAlMo thin coatings obtained by magnetron sputtering

Y.Y. Santana [a,*], M.A. Sow [b], C. Nouvellon [c], C. Cordier [b], F. Beclin [b], M. Touzin [b], A. Tromont [c], X. Noirfalise [c], L. Boilet [d], J.F. Trelcat [d], M. Dubar [a], H. Morvan [a], M. Bigerelle [a]

[a] Univ. Polytechnique Hauts-de-France, LAMIH, CNRS, UMR 8201, F-59313 Valenciennes, France
[b] Univ. Lille, CNRS, INRAE, Centrale Lille, UMR 8207 - UMET - Unité Matériaux et Transformations, F-59000 Lille, France
[c] Materia Nova Research Center, Avenue Copernic 3, 7000 Mons, Belgium
[d] Belgian Ceramic Research Centre, 7000 Mons, Belgium

ARTICLE INFO

Keywords:
High entropy alloys
Thin coatings
Powder target sintered
Magnetron sputtering
Reciprocating dry sliding wear
Nanoindentation

ABSTRACT

High Entropy Alloys of FeCrMnAlMo thin coatings obtained by magnetron sputtering were studied. The influence of the powder mixing method to obtain the targets used in the physical vapor deposition reactors was evaluated concerning the mechanical and tribological properties of the coatings. The microstructural characterization was also performed. The high purity element powders of 34Fe-22Cr-19Mn-19Al-6Mo were mixed in two ways: mechanically alloyed for 35 h (MS coating) and the other by conventional mixing for 30 min (CM coating). The coatings showed a poorly crystallized structure, almost amorphous. X-ray photoelectron spectrometry results evidenced that the MS coating contains approximately 8 at.% C, while no carbon was detected in the CM coating. The coatings presented hardness values determined by nanoindentation of ~8.7 GPa and 7.4 GPa for MS and CM coatings, respectively. A better reciprocating dry sliding wear resistance with specific wear rate (k) of ~3.33×10^{-5} $mm^3\ N^{-1}\ m^{-1}$ for MS coating/substrate system was found, while for the CM coating/substrate system was of ~8.23×10^{-5} $mm^3\ N^{-1}\ m^{-1}$. The abrasive wear mechanism was observed with the formation of ploughing, scratching and debris wear adhered to the alumina counterpart ball.

1. Introduction

High entropy alloys (HEA) were first reported in studies conducted in 2004 by Yeh et al. [1] and Cantor et al. [2]. These alloys were designed taking into account the rule of maximum entropy configuration and consisted of five to more elements with concentrations ranging from 5 at.% to 35 at.%. The single-phase solid solutions of fcc, bcc, or hcp are found due to their high entropy of mixing [3]. HEA in bulk form have been mainly studied because they combine strength and ductility, high corrosion resistance, and high wear resistance [4–8]. The hardness of HEA bulk alloys can vary between HV ~2 GPa (CoCrFeNiCu) to HV ~8 GPa (MoTiVFeNiZrCoCr), according to Zhang et al. [4]. Ayyagari et al. [6], have studied bulk alloys of CoCrFeMnNi and $Al_{0.1}$CoCrFeNi; finding hardness ($HV_{2.94N}$) values of ~1.31 GPa and 1.52 GPa, respectively. Also, for 1 N and 1800 s was determined the specific wear rate of ~7.4×10^{-4} $mm^3\ N^{-1}\ m^{-1}$ and ~1.9×10^{-4} $mm^3\ N^{-1}\ m^{-1}$, respectively. Other $CoCrFeNiMo_{0.2}$ HEA bulk was tested on reciprocating sliding wear by Deng et al. [8], obtaining the specific wear rate of ~0.52×10^{-3} $mm^3\ N^{-1}\ m^{-1}$ to a normal load of 5 N after 600 cycles.

However, the high cost of the raw material, the difficulty of producing bulk HEA by casting, and the concern for improving mechanical and tribological properties lead us to explore new applications such as HEA coatings [4,5,9]. Among the coating's deposition techniques, magnetron sputtering is widely used method for thin-film processing. A wide range of compositions and easier microstructure control can be achieved with various process parameters [9,10]. High entropy alloys magnetron sputtering films can be obtained by powder target [11] or multi-target [12]. Powder target can be made by mixing powders with the desired composition which allows more control of the coating composition and reduction of the number of magnetrons to one

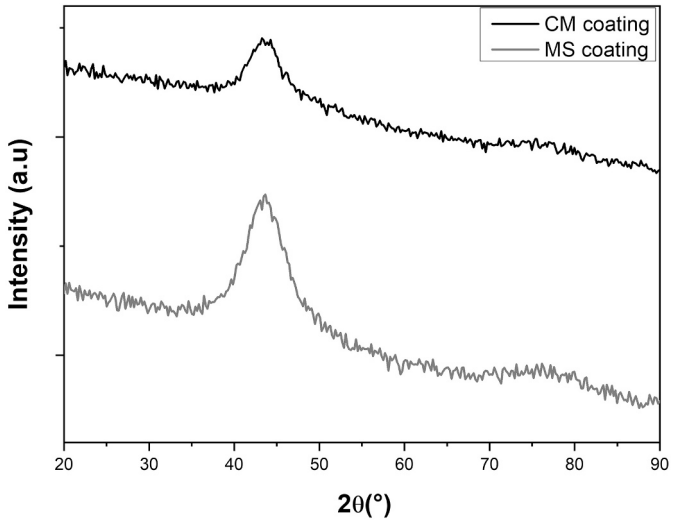

Fig. 1. XRD pattern of FeCrMnAlMo PVD thin coatings collected at 0.8° of incidence angle.

[11,13,14].

It has been widely studied that the relationships between hardness and modulus of elasticity (H/E, H^3/E^2) can be correlated to the tribological behavior of materials [15–17]. The H/E corresponds to the elastic strain to failure and the H^3/E^2 is correlated to the ability to resist plastic deformation. Hence the importance of coatings fabrication with high hardness values and low elasticity modulus values.

Thus, the PVD technique allows obtaining HEA thin coatings with high hardness values due to the high residual stresses and nanocrystalline structure [9,18–20]. Studies on CoCrFeMnNi nanocrystalline thin coatings obtained by RF magnetron sputtering showed a hardness of ~6.8 GPa [20]. Sha et al. [18] have obtained FeMnNiCoCr PVD coatings with hardness values between 7 GPa and 9 GPa by nanoindentation. Also, it was found in $CoCrFeMnNiAl_x$ and $CoCrFeMnNiTi_x$ the hardness varied between 6 and 9 GPa [21]. The formation of nanocrystalline structure and preferred growth orientation of the sputtering PVD films produced high hardness values (10–12 GPa) [22]. Zendejas Medina et al. [23] studied thin films of CrMnFeCoNi by magnetron sputtering with hardness values between 8 and 12 GPa.

On the other hand, few works on the tribological performance of HEA PVD coatings have been realized despite their great importance for industrial applications. The tribological performance of (FeMnNiCoCr)N_x HEA coatings obtained by sputtering onto M2 steel substrates were evaluated by Sha et al. [17]. They found that coatings with nitrogen content up to 6 at.% had fcc structures with a hardness of 11 GPa and presented good adhesion and wear resistance (k ~1.4 × 10^{-6} mm^3 N^{-1} m^{-1}).

In this work, we will study the influence on microstructural, mechanical and tribological behavior of powder mixed process to obtain powder target sintered to deposit FeCrMnAlMo HEA coatings onto a low-carbon steel substrate. The powder targets sintered were obtained of the same composition either produced from elementary powders mixed by a mechanically alloyed process or produced by a conventional mixed. This composition was selected because it has been previously synthesized by the mechanically alloyed technique and it was obtained that it forms a bcc structure that presents greater hardness and mechanical resistance [24].

2. Experimental details

Two powder mixtures of composition (at.%) 34Fe-22Cr-19Mn-19Al-6Mo have been prepared from high purity (~99 %) elemental powders of different particle size: Al (<15 μm), Cr (38–45 μm), Fe (<60 μm), Mn (<45 μm) and Mo (<350 μm). The first powder was prepared with mechanically alloyed powders (for MS target). The milling was performed in a RETSCH PM- 100 planetary mill with six small balls of 10 mm and three large balls of 20 mm in diameter [24]. The jar and the balls are made of stainless steel. The assembly (jar + balls + powder) is maintained under an inert atmosphere (Argon) to prevent oxidation. The ratio of ball mass to powder mass was 10:1 and the actual milling time was 35 h at a speed of 450 rpm. Breaks of 15 min were scheduled after every 30 min to prevent heating during milling. In addition, 2 wt% stearic acid ($C_{18}H_{36}O_2$) was added to limit excessive powder welding to the jar and balls. The second powder (for CM target) was obtained by conventional mixed; the elemental powders were dry milled for 30 min in a Turbula mixer (balls and container of stainless steel).

Both mixtures were then consolidated by commercial Spark Plasma Sintering equipment (HPD10, FCT GmbH). Around 35 g of powder was put in a 5.08 cm diameter graphite mold. The processing cycle consisted of three steps under vacuum: rapid heating at 50 °C/min up to 1000 °C (force of 62 kN applied from the beginning of the cycle), a 5 min dwell time, and rapid cooling up to room temperature. After consolidation, both faces of the targets were rectified to eliminate the eventual surface contamination due to the graphite tooling and surface roughness. The final thickness of the targets is around 2.5 mm. The final composition of the targets was controlled by X-ray fluorescence measurement; the

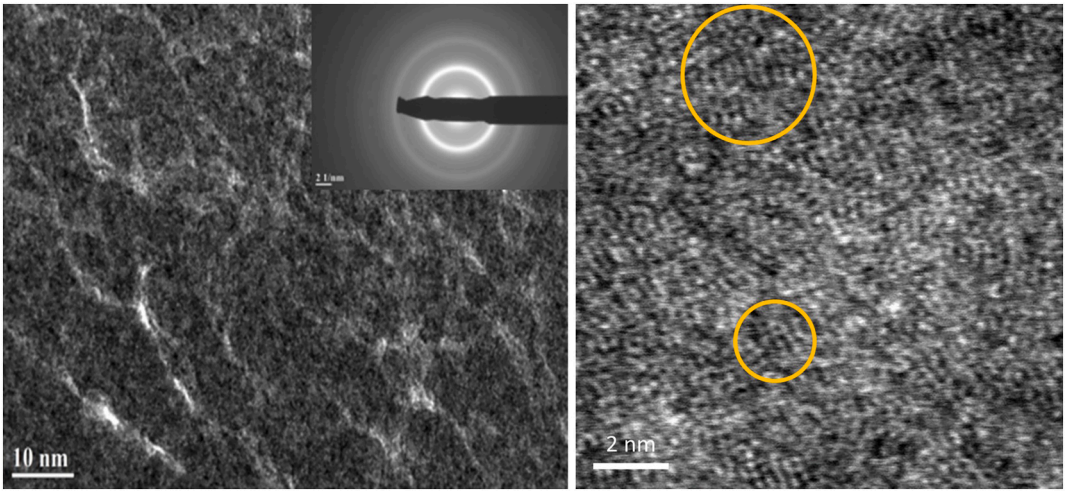

Fig. 2. TEM images of MS coating and deposited on silicon wafer Si (100): (a) Dark-field (DF) and the corresponding Selected Area Electron Diffraction (SAED) pattern, (b) HRTEM (HAADF).

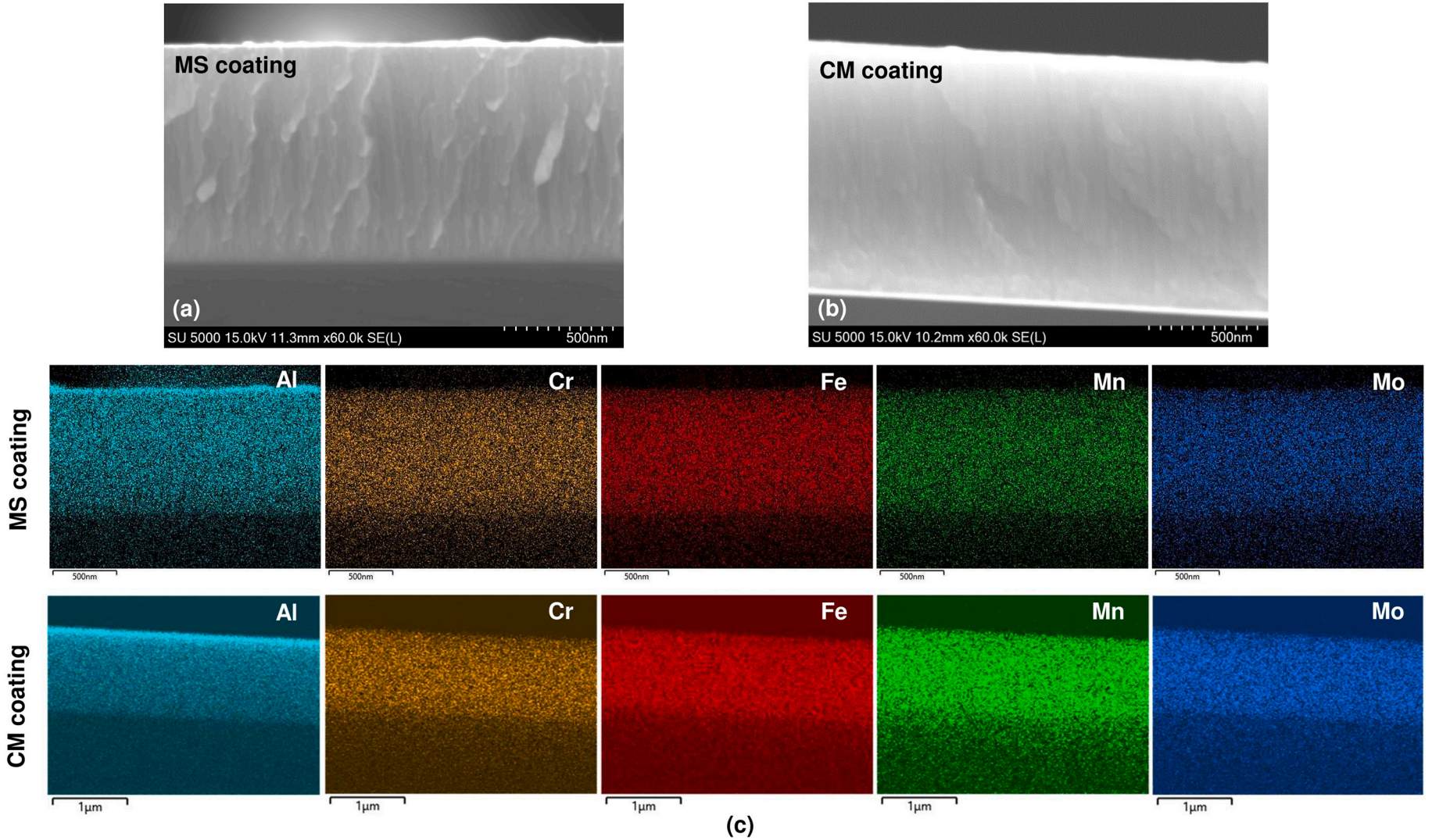

Fig. 3. Morphology of the FeCrMnAlMo PVD thin coatings onto Si wafers obtained by SEM: (a) MS coating and (b) CM coating and (c) EDS analysis.

Table 1
Chemical composition by EDS of elements of targets and coatings of HEA FeCrMnAlMo.

Material	Chemical composition (at.%)				
	Al	Cr	Fe	Mn	Mo
MS Coating	17.9 ± 0.4	21.6 ± 0.6	36.0 ± 0.6	18.1 ± 0.8	6.4 ± 0.3
MS target	17.5 ± 0.2	21.7 ± 0.5	34.9 ± 0.4	19.9 ± 0.1	6.0 ± 0.1
CM Coating	18.4 ± 0.4	21.8 ± 0.2	33.7 ± 0.3	20.1 ± 0.2	6.0 ± 0.3
CM target	19.5 ± 0.4	18.8 ± 0.5	35.4 ± 0.8	20.6 ± 0.7	5.8 ± 0.2

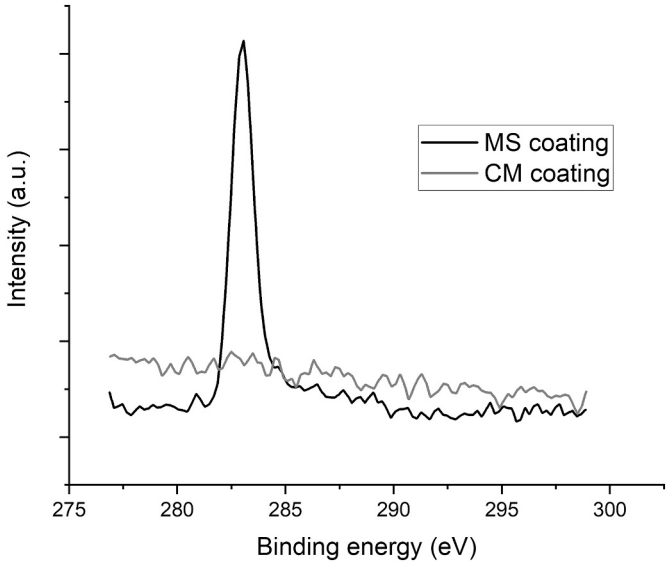

Fig. 4. Core-level XPS C1s spectra for the FeCrMnAlMo PVD thin coatings.

Table 2
Mechanical properties of FeCrMnAlMo PVD thin coatings.

Coating	H (GPa)	E_r (GPa)	H/E_r	H^3/E_r^2 (GPa)
MS	8.7 ± 0.3	180 ± 6	0.048	0.020
CM	7.4 ± 0.3	173 ± 6	0.043	0.014

deviations were compared to the initial composition obtaining values <1 at.%.

The FeCrMnAlMo HEA thin coatings were synthesized by magnetron sputtering in a cylindrical stainless steel chamber. The chamber is evacuated down to a residual pressure of 1.6×10^{-6} to 4.6×10^{-6} mbar employing a dry primary pump combined with a turbo-molecular pump. An unbalanced magnetron cathode was located on the side of the chamber, where a target of 5.08 cm in diameter and 2.5 mm thick was sputtered in Ar gas with a constant total flow rate of 77 sccm (standard cubic centimeter per minute). The working pressure was fixed at 1 Pa by using a throttle valve. The target/substrate distance was fixed at 9 cm. The target alloy was sputtered in DC mode by an Advanced Energy MDK 500 power supply. The power was fixed at 60 W, corresponding to a power density on the target surface of 3 W/cm^2 which was calculated using the target area exposed to the plasma of ~20 cm^2. The MS and CM coatings were obtained with MS and CM targets, respectively. The surface roughness (Sa) was approximately 0.002 μm for both coatings. Silicon wafer substrates were used to allow thickness measurement, chemical composition, structure analysis and morphological characterization, while polished steel (SAE 1015) substrates of surface roughness (Sa) ~0.003 μm were used for the nanoindentation and tribological study. The thickness of the coatings of ~1.0 ± 0.1 μm is obtained by a mechanical profilometer (Veeco, Dektak 150), measuring the step between a coated and an uncoated zone.

The structures of the coatings deposited on Si substrates were analyzed by grazing incidence X-ray diffraction (Empyrean Cu LFF HR (9430 0337310×) DK419664) with Cu kα radiation (λ = 1.54183 Å) and operated at 45 kV and 20 mA. The scan angle (2θ) was between 20 and 90°, and the incidence angle was 0.8°. An additional structural study of the MS coating was carried out by high-resolution transmission electron microscopy (HRTEM). Two microscopes were used (the FEI Tecnai G2–20 twin TEM at 200 kV and the FEI Titan Themis TEM at 300 kV). The samples were roughly polished on the substrate side by SiC papers (P800 and P4000) to reduce the thickness of samples down to about 50 μm. Subsequently, samples were glued to a copper TEM support grid. Final thinning was performed using ion mill-Gatan Duo Mill. The coatings were observed in plane view. Also, the microstructure of the cross-section was observed by scanning electron microscopy (SEM) and the chemical analysis was performed by energy dispersive spectroscopy (EDS).

The carbon content of the coatings was analyzed by X-ray photoelectron spectroscopy (XPS) using an ESCA-5000 (Physical Electronics) Versa Probe system. The data were collected using monochromatic Al k_α radiation source with a photon energy of 1486.6 eV. The following X-ray settings were used: beam size diameter: 200 μm; beam power: 50 W; voltage: 15 kV. The pressure in the analysis chamber was typically 2×10^{-6} Pa. Photoelectrons were collected at a take-off angle of 45° (normal detection) from the normal surface. A compositional profile was made for two coatings samples with argon sputtered (Ar^+ 2 kV sputtered area: 2 × 2 cm^2). The profiles were performed with a step of 25 nm until rising 500 nm in depth. At each step, the elements were analyzed with a pass energy of 23.5 eV (high-resolution spectra) and an energy step of 0.2 eV. The resolution of the XPS apparatus is estimated to be 0.5 eV. Atomic compositions were derived from peak areas after a Shirley background subtraction using photoionization cross-sections calculated by Scofield, corrected for the dependence of the escape depth of the kinetic energy of the electrons, and corrected for the analyzer transmission function of our spectrometer.

Mechanical properties such as hardness and reduced elastic modulus were determined using a Hysitron Triboindenter (TI980, USA). The nanoindentation tests with a diamond Berkovich indenter were carried out using a quantitative ultra-high-speed mechanical property mapping (XPM). This technology can perform six measurements/s. The testing was conducted on the coatings deposited on a steel substrate. For each coating, three indentations arrays of 15 × 20 (858 indents) were performed to a maximum load of 2 mN to guarantee a penetration depth of <10 % of the coating thickness. The spacing between indentations of 2 μm (i.e., 10–20 times the indentation depth) was left [25]. The hardness and elastic modulus were determined using the standard Oliver and Pharr method [26]. Also, with this equipment, the adherence of the coating to the substrate was evaluated by progressive load nanoscratch testing (F_N: 5 mN to 500 mN). For this purpose, six nanoscratch test for each coating were realized, a conical diamond indenter with a radius tip of 20 nm was used. The displacement rate of 0.02 mm/s and the scratch distance of 1 mm were applied. Lateral force (F_L) and friction ($F = F_L/F_N$) were collected as a function of lateral displacement. The depth profile and the 3D image of scratch tracks were obtained using the optical profilometer at 20×.

The tribological behavior was evaluated by reciprocating dry sliding wear tests using a pin-on-disc configuration in the Tribolab UMT (Bruker, USA). Three tests for each coating were carried out at room temperature with a 12 mm diameter Al_2O_3 ball. The test parameters were: a stroke length (L) of 2 mm, a normal load of 1 N, a wear time of 1000 s (2500 cycles), a sliding distance of 10 m and a sliding velocity of 10 mm/s. The wear track in the sample coated and the balls were observed by SEM and EDS. The wear track cross-sectional area (A) in mm^2 was measured with the optical profilometer. The volume loss (V_L in mm^3), representing the volume of material removed by wear, was determined by:

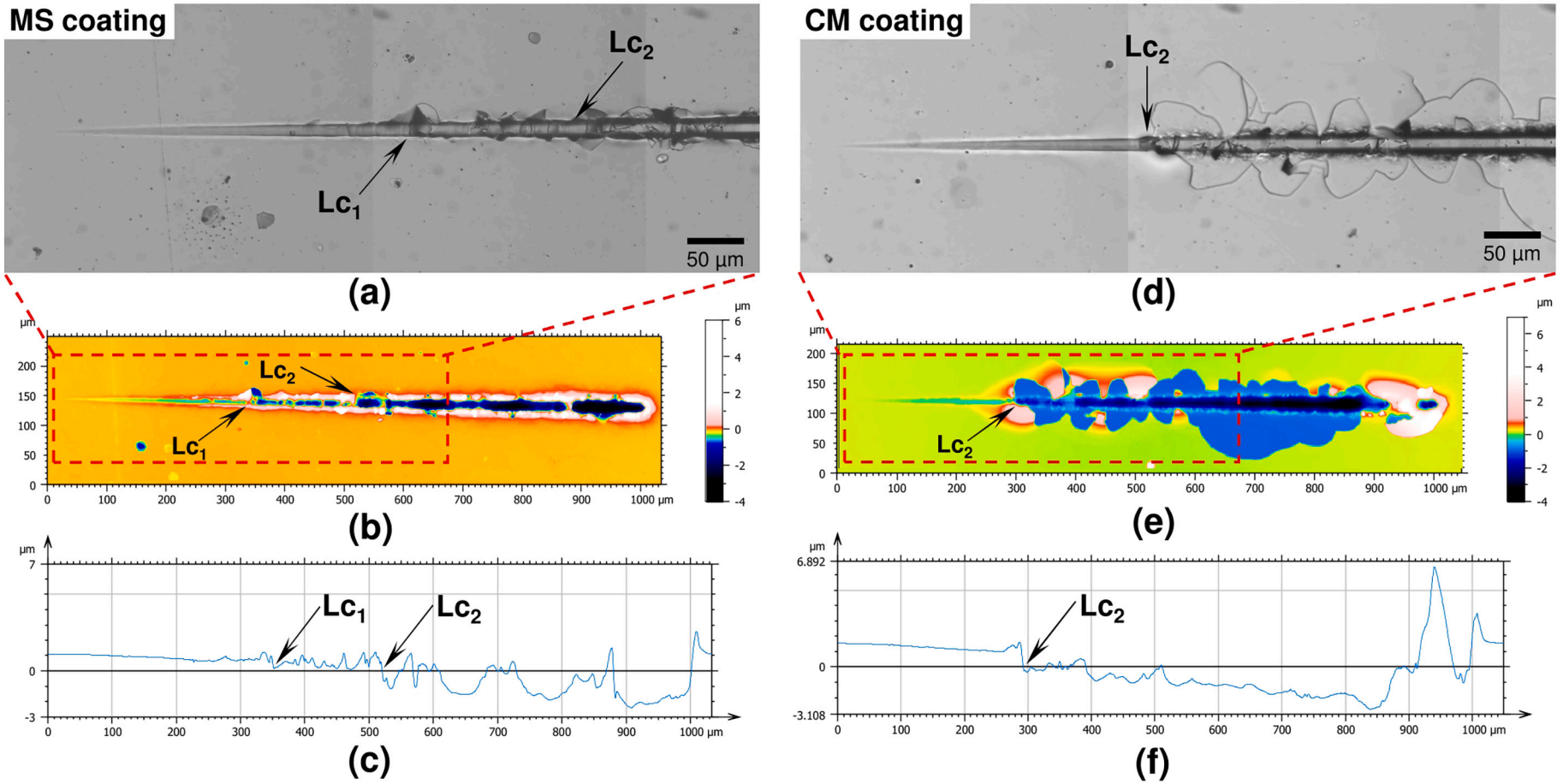

Fig. 5. Results of nanoscratch track observations for MS coating (a), (b) and (c) and CM coating (d), (e) and (f): image by MO (a) and (d), 2D optical profilometry (b) and (e), and curves of penetration depth of the scratch (c) and (f).

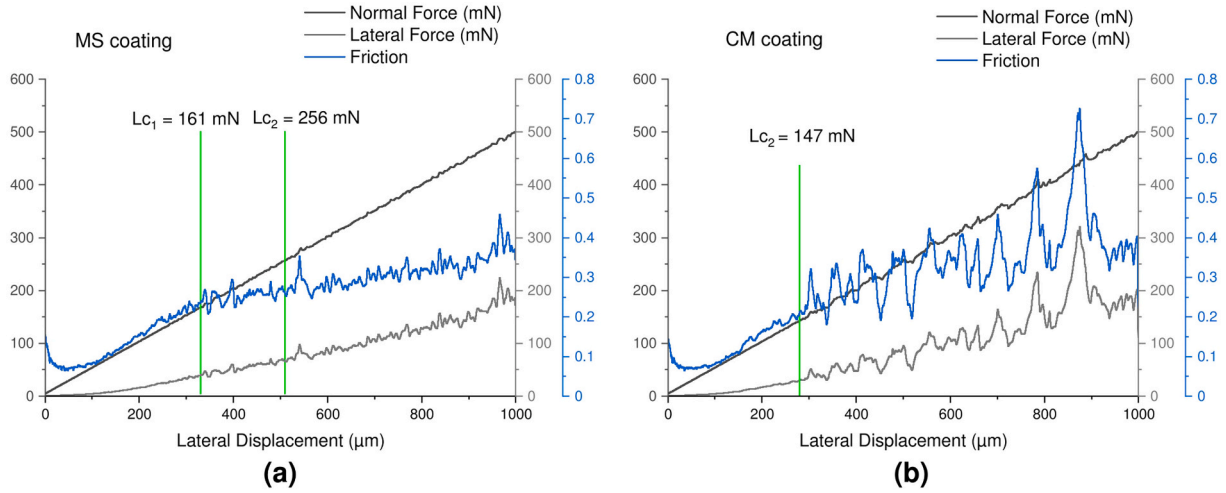

Fig. 6. Graphics of normal force, lateral force, and friction vs. displacement for scratch tests on the coatings: MS (a) and CM (b).

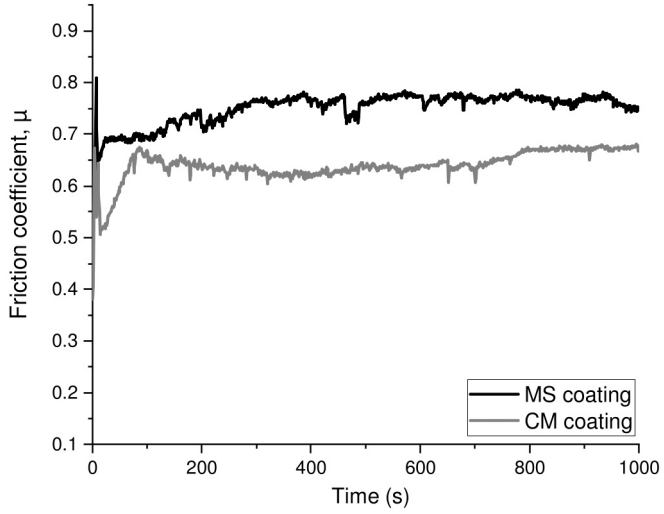

Fig. 7. Curves of the friction coefficient as a function of time for FeCrMnAlMo PVD thin coatings tested against Al_2O_3 balls.

$$V_L = AL \tag{1}$$

The Archard wear coefficient (K) was determined by the equation:

$$Q = KW/H \tag{2}$$

where Q is the volume of material removed from the surface by wear per sliding distance unit (V_L/S), W *[N]* is the normal load applied between the surfaces, and H *[GPa]* is the hardness of the softer surface. The constant K (Archard wear coefficient) is dimensionless and always less than unity. K provides a way of comparing the severities of different wear processes [27]. However, for engineering applications the specific wear rate (k) is more useful. The quantity $k = K/H$ [mm^3N^{-1} m^{-1}] represents the volume loss (V_L) per sliding distance unit per normal load unit on the contact [27].

3. Results and discussion

3.1. Structural and microstructural characterization

The XRD patterns of the MS and CM coatings are shown in Fig. 1. Both coatings revealed one broad peaks at $2\theta = 43.66°$. The inter-reticular distance corresponding to the peak at 43.66° is $d_{hkl} = 2.07$ Å. These broad peaks indicate that the films are very poorly crystallized, almost amorphous [19,28,29]. The structure of MS coating was also analyzed by a high-resolution TEM image (HRTEM). Fig. 2a shows a representative TEM image and the corresponding Selected Area Electron Diffraction (SEAD) pattern of MS coating. It was noted that the electronic diffraction pattern exhibits at least two visible broad rings. The inter-reticular distance corresponding to these rings is respectively $d_1 = 2.07$ Å and $d_2 = 1.2$ Å, confirming the XRD results. Fig. 2b shows the HR-TEM image. It confirms that the structure is very poorly organized but it is nevertheless possible to observe successions of a few atomic planes in certain areas (in yellow circles). This type of structure is expected for this mode of deposition. Indeed, the formation of the coating takes place at almost room temperature. Atomic diffusion is therefore too weak for the atoms to be able to organize themselves into a crystalline structure.

The coatings morphology characterization was performed by SEM. The fracture cross-section of the coatings onto Si-wafer is shown in Fig. 3a and b; a columnar growth could be observed for both coatings. The chemical composition determined by EDS is presented in Table 1, the results show a slight composition variation compared to the target. Also, it could be observed in the EDS mapping analysis that the coatings presented a homogeneous composition through the thickness (Fig. 3c).

The carbon contents of the coatings were determined by the XPS technique, the surface was bombarded with Ar + ions every 25 nm to a depth of 500 nm, the atomic carbon percentage values obtained were averaged. For the MS coating is obtained ~8 at.% C, which was possibly added to the alloy during the mechanical alloying process of powder target by adding 2 wt% stearic acid ($C_{18}H_{36}O_2$). For the CM coating, no carbon was found by this technique. Fig. 4 shows the average curves of core-level spectra of Cs1 for both coatings, a peak at ~283 eV was found for MS coating; typical binding energy for a metal carbide formation or carbidic environment in amorphous Me-C films [30,31]. After the first layer was removed, no free carbon was found. XPS analysis cannot distinguish the nature and bond strength of carbon in metal carbide and in solid solutions [31]. Also, the results of XRD and TEM analysis could not confirm the presence of carbide. Indeed, it is possible that the carbon is in the form of carbide very small and localized at the grain boundaries or in the supersaturated solid solution. Also, as has been reported by other researchers [31–34], the sputter deposition process limits the mobility of the atoms due to rapid cooling, which would hinder the formation of carbides larger unit cells. Therefore, as the high entropy alloy exhibits lattice distortion due to a large number of metallic elements, it may result in a wider range of interstitial site sizes. In this sense, these researchers have found that thin coatings obtained by PVD sputtering can have a higher carbon solubility leading to supersaturated solid solutions.

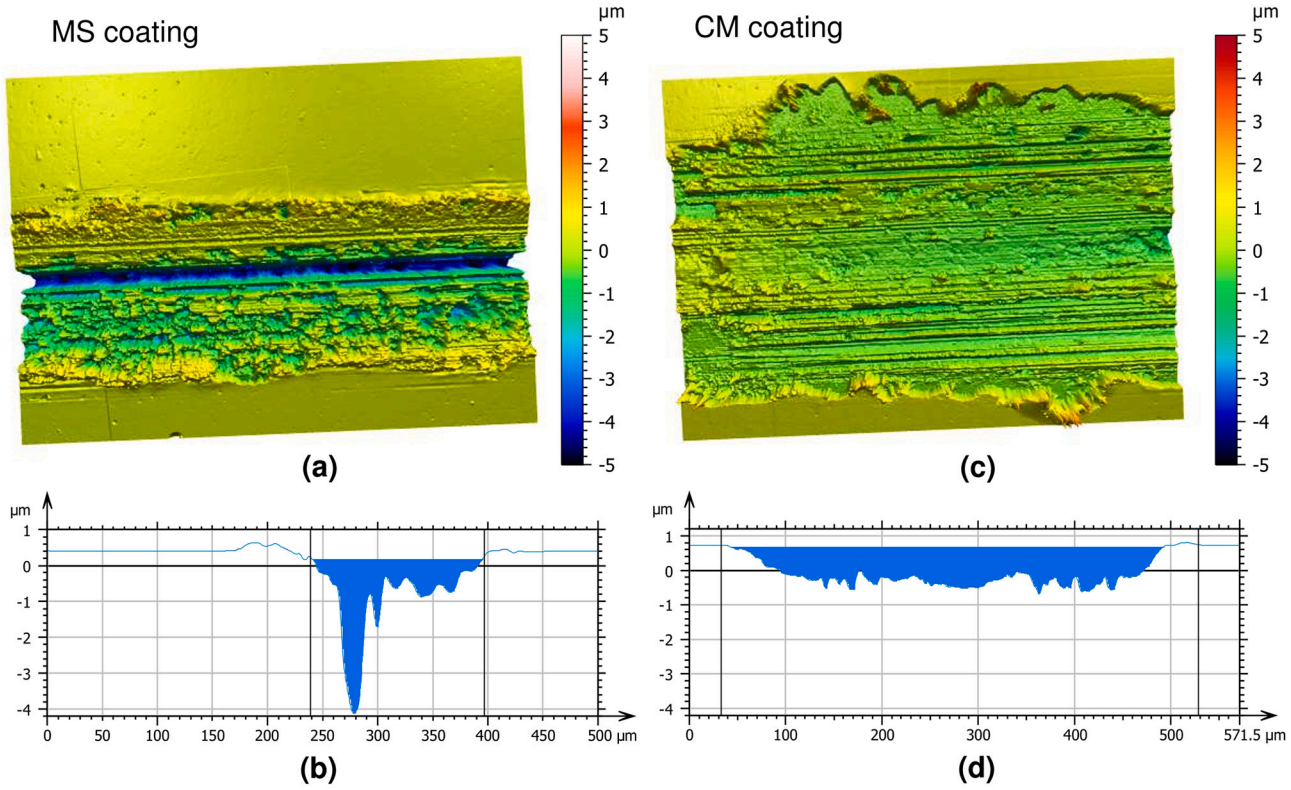

Fig. 8. Topography of wear tracks by optical profilometry for the MS coating (a) and (b) and for the CM coating (c) and (d): wear track 3D-image (a) and (c) and sectional wear track profiles (b) and (d).

3.2. Mechanical and tribological characterization

The mechanical properties of the FeCrMnAlMo PVD thin coatings are presented in Table 2. The hardness (H) for the MS coating is 8.7 GPa and for the CM coating is 7.4 GPa while the values of the effective elastic modulus (E_r) are similar for both coatings. Typically, the sputtering process generates thin coatings with higher hardness due to the high levels of compressive residual stresses that originate during the deposition of the atoms on the surface. Similar hardness values were obtained for other HEAs PVD coatings with different chemical composition, studies by Dang et al. [20] and Sha et al. [18]. The higher hardness of the MS coating could be attributed to the presence of carbon in the supersaturated solid solution producing a higher lattice distortion than the non-carbon lattice as it is for the CM coating, such as has been reported in other works [31,34].

In addition, the tribological characterization was conducted by the adherence and reciprocating dry sliding tests. The coatings adherence results are showed in the Figs. 5 and 6. Fig. 5 presents the micrograph by optical microscopy, 2D image and the linear profile by optical profilometry of a representative test for each coating. Additionally, normal force (F_N), lateral force (F_L), and Friction (F) have been recorded as a function of the lateral displacement (Fig. 6). The critical loads (Lc_1 and Lc_2) were determined from a combined analysis based on the graph of F_N, F_L, and F (Fig. 6), optical microscope images and the profilometry scratch track (Fig. 5). Lc_1 is used to indicate the first cracking or partial spallation, and Lc_2 is the load for which the complete failure of the coating occurs, i.e., exposure of the substrate [17,35].

For the MS coating obtained from the mechanically alloyed powder, a first failure or local spalling (Lc_1) was observed at an average load of 161 mN, corresponding to a scratch distance of 330 µm. Then, the complete removal of the coating was observed at an average load of 256 mN (scratch distance of ~510 µm); this load was then taken as the critical load Lc_2. For the CM coating produced with a mixture of commercial powders, the critical load Lc_1 could not be identified; only the critical load Lc_2 could be quantified with a value of ~147 mN for a scratch distance of ~280 µm. These critical load values correspond to significant variations in friction (Fig. 6).

Besides, both coatings exhibited different delamination modes. For the CM coating, the observed adhesive failure mode corresponded to a brittle failure mode called "compressive spallation" [35]. This failure mode produces chipping in the trackside, i.e. the formation of semi-circular cracks that propagate to the sides of the centerline of the track occurs, as observed in Fig. 5d and e. Conversely, a ductile failure mode denominated "spallation" was observed for the MS coating. Lower crack areas characterize this delamination, i.e. smaller chipped or spalled regions [35]. Based on these characteristics, it was observed that the MS coating showed better adhesion than the CM coating. The scratch behavior can also be analyzed based on the mechanical properties. The better adhesive behavior of the MS coating compared to the CM coating could be correlated to its higher values of H, H/E_r and H^3/E_r^2 (Table 2); these parameters indicate a higher ability to resist plastic deformation, cracking damage, and gross spallation for the MS coating. These correlations between mechanical properties and the adhesion performance have also been found in other HEA PVD coatings [17].

Figs. 7-11 and Table 3 show the reciprocating dry sliding wear test results. The evolution of friction coefficients as a function of time is shown in Fig. 7. A wear running-in, where the friction coefficient increases progressively, is present until approximately 90 s for CM coatings and then the friction coefficient reaches a specific value approximately constant. For MS coating could not be observed the running-in. The average friction coefficients (μ_p) in the constant zone are presented in Table 3. The friction coefficient of MS coating is slightly higher than the CM coating. It is widely studied that the friction coefficient depends on the microstructural characteristics, mechanical properties of the coating, and the changes between the wear surfaces during sliding, such as the formation of oxide debris and cracks [7,8,36].

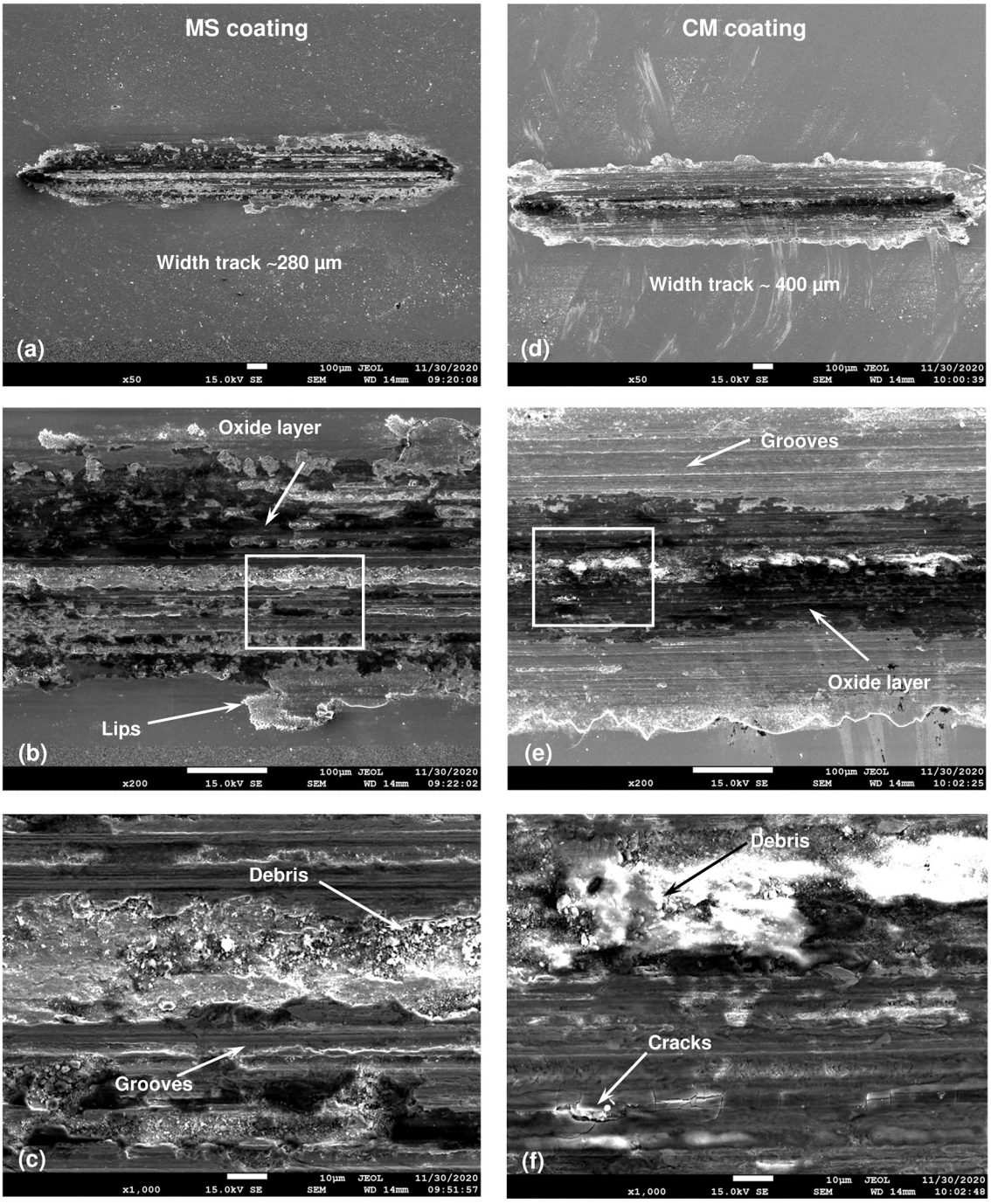

Fig. 9. Morphology of wear tracks by SEM for MS and CM coatings.

In the case of the coatings under study, the microstructural features and roughness surface are similar; both coatings are poorly crystalized but differ in chemical composition. As presented above, the MS coating contains 8 % at. C and the CM coating does not. Also, the MS coating presents a higher hardness than the CM coating (Table 2). Therefore, it could be presumed to be responsible for the difference in the friction coefficient. Additionally, this difference could be explained on the basis of rapid wear of the coating due to low adherence to the substrate resulting in delamination failure of the CM coating. The average friction coefficient ($\boldsymbol{\mu}_p$) for CM coating/substrate system is close to the values found in a sliding contact between alumina and steel ($\boldsymbol{\mu}_p$ ~0.60–0.65) [37]. Besides, it could be observed that the curves of the friction coefficient as a function of time showed slight fluctuations. According to several studies [7,8,36], the fluctuations during the test can be attributed to the presence of wear debris formed and accumulated in the wear track, to the formation of oxide patches and localized fractures, which will be confirmed later in this study.

Regarding the determination of the wear volume loss (V_L), the wear tracks were evaluated after removing the debris with an air jet, 3D and 2D profilometry images, and average wear profiles were obtained along the length of the track without considering the edges of approximately 100 µm on each side. Fig. 8 shows the representative wear track of three tests performed for each coating. The volume loss (V_L) was determined by the average of the cross-sectional areas of the wear track (blue zone in the profiles of Fig. 8b and d), multiplied by the stroke length of 2 mm. The results of the specific wear rate (k) and Archard's wear coefficient

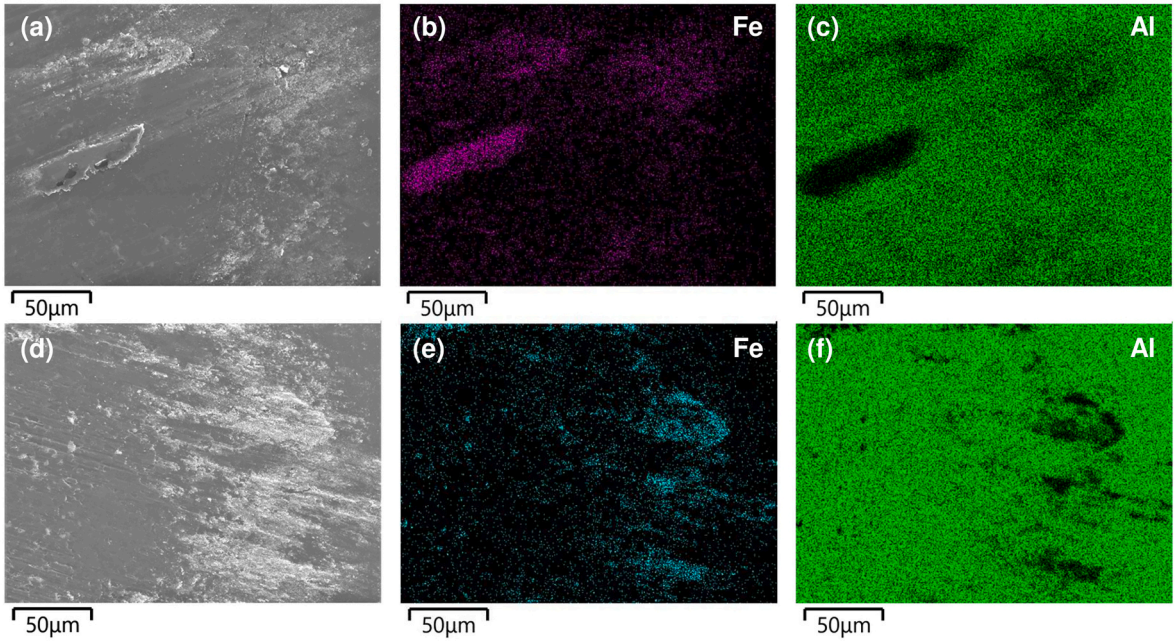

Fig. 10. Micrography and EDS mapping analysis of the wear track on Al_2O_3 counterparts tested against MS coating: (a), (b), (c) and CM coating: (d), (e), (f).

(K) are presented in Table 3. It was found that CM coating/substrate system presented a volume loss and a specific wear rate of 147 % higher than MS coating/substrate system. Concerning Archard's wear coefficients, values in the order of 10^{-4} were computed for both coatings/substrate system, close to the transition limit from mild to severe wear for unlubricated sliding [38].

On the topographic analysis presented in Fig. 8, it can be observed that the wear tracks show pronounced grooves parallel to the sliding direction. This morphology is more accentuated for CM coating/substrate system with a maximum wear track depth value of ~1.2 μm and width wear track of ~400 μm, indicating that the wear barely reached the substrate. For MS coating/substrate system, a less-width wear track of ~280 μm was determined; a narrow groove of ~4 μm in depth was also observed, possibly formed by wear debris detached from coating material and adhering to the ball, as will be shown later. Regarding the linear cross-sectional profile of the wear tracks of the MS coating/substrate system, 75 % of the wear track have a maximum depth of ~1.2 μm, which could indicate that the MS coating was progressively worn until it reached the substrate.

Details of the morphology of the wear track can be observed in the Fig. 9. For both coatings/substrate system, it can be observed the grooves characteristics of scratching and ploughing. Deep grooves were produced from wear debris that subsequently adhered to the pin, as evidenced in the SEM-EDS analysis of the wear track for the Al_2O_3 balls presented in Fig. 10. Also, for both coatings/substrate system, the presence of fine debris wear and dark regions with cracks are observed at higher magnification (Fig. 9). Based on EDS analysis of the wear tracks shown in Fig. 11, the presence of oxygen was observed preferentially throughout the wear track for the MS coating/substrate system and the CM coating/substrate system, indicating that the tribo-oxide layer (dark regions in Fig. 9b and e) formation was possible during the test. The oxidation occurs on the worn surface heated by friction and deformation. The characteristics mentioned above are predominant in abrasive wear mechanisms. Similar wear mechanisms have been observed in other HEA coatings [17] and HEA bulks [7,39].

The reciprocating dry sliding wear behavior can also be related to the ratios of mechanical properties presented in Table 2, where MS coating shows higher values of H/E_r (related to the elastic strain to failure) and H^3/E_r^2 (related to the ability to resist plastic deformation) than the CM coating; which is consistent with its better wear behavior.

4. Conclusions

The microstructural, mechanical and tribological characterization of HEA thin coatings onto low carbon steel obtained by magnetron sputtering were studied using two different powder mixing methods to produce targets used in a magnetron sputtering reactor. Both FeCrMnAlMo HEA thin coatings presented a poorly crystallized structure. The coatings showed a dense columnar microstructure and a homogeneous composition. Chemical analysis revealed the presence of carbon in the MS coating (8 at.% C) obtained with the target fabricated from powder mechanically alloyed. Since no carbon was detected in CM coating, it is thought that its presence in the MS coating is due to the use of stearic acid during the mechanical mixing. It is also believed that the carbon may be in the supersaturated solid solution and in the form of carbide nanocomposites, which may be responsible for the higher hardness value of the MS coating.

The tribological performance of the HEA PVD coatings/substrate system was established by adherence and reciprocating dry sliding wear studies. The adherences results showed different mechanisms of delamination; a ductile failure mode for MS coating/substrate system with a higher critical load of delamination showed enhanced adherence to the substrate, contrary to CM coating/substrate system that presented a brittle failure mode of delamination with a lower critical load. The Archard's wear coefficient determined was in the order of 10^{-4} for both coating/substrate systems and the specific wear rate for MS coating/substrate system was 147 % lower than for CM coating/substrate system. Therefore, it was found that the better wear resistance of the system MS coating/substrate is due to both better adherence to the substrate, a higher hardness values and higher H/E_r and H^3/E_r^2 ratios. The wear mechanism found was the abrasive type with material transference from the sample to the pin. In further work, we envisage the study of coatings with improved hardness from conventionally mixed powders with variations of the deposition condition to discern if the enhanced tribological behavior of these coatings is directly correlated to an improvement in the hardness of the coatings.

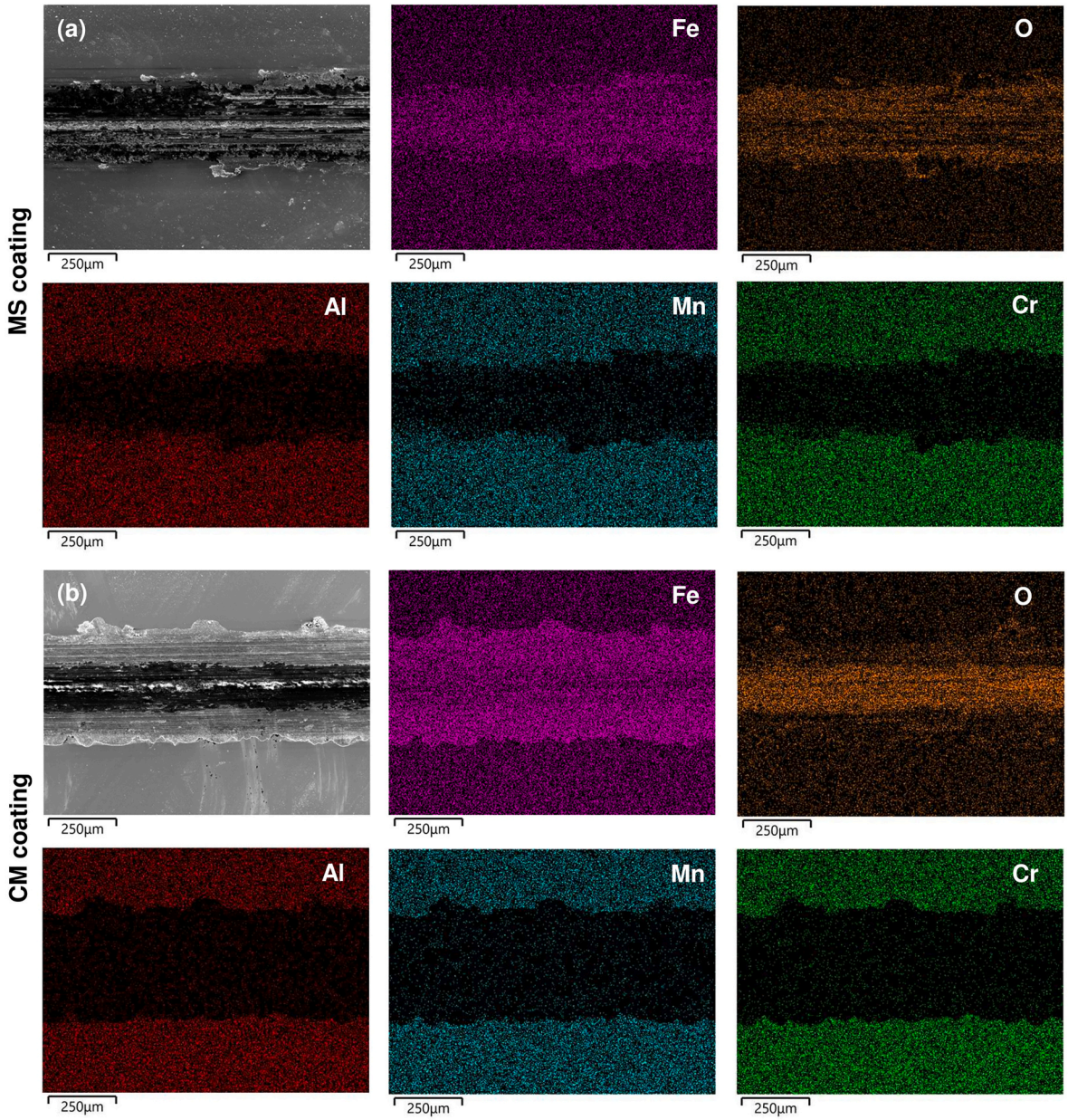

Fig. 11. Micrography and EDS analysis of wear tracks on the MS and CM coatings.

Table 3
Tribological results FeCrMnAlMo PVD thin coatings.

Coating	V_L (mm^3) × 10^{-4}	k (mm^3N^{-1} m^{-1}) × 10^{-5}	K × 10^{-4}	μ_p
MS	3.33 ± 0.56	3.33 ± 0.19	2.88 ± 0.16	0.763 ± 0.018
CM	8.23 ± 0.21	8.23 ± 0.07	6.11 ± 0.05	0.643 ± 0.026

CRediT authorship contribution statement

Y.Y. Santana: Methodology, Data analysis, Investigation, Writing-original draft, Writing - review & editing. **M.A. Sow:** SEM and TEM observations, Writing - review & editing. **C. Nouvellon**: Project administration, Review & editing, **C. Cordier**: Supervision, review & editing, **F. Beclin:** Supervision, review & editing, **M. Touzin**: Review & editing, **L. Boilet:** Review & editing. **A. Tromont**: PVD coating preparation, **X. Noirfalise**: XPS analyses, **M. Dubar**: Review & editing, **H. Morvan:** Data curation, **J.F. Trelcat**: Targets' fabrication. **M. Bigerelle**: Supervision, review & editing.

Declaration of competing interest

The authors declare that they have no known competing financial interests or personal relationships that could have appeared to influence the work reported in this paper.

Data availability

The authors do not have permission to share data.

Acknowledgements

This work is supported by the Department of the Research Programs of the DGO6 (Wallonia) and the Fonds Européen de Développement

Régional (FEDER) through the INTERREG V France-Wallonie-Vlaanderen program “Allihentrop”. The Chevreul Institute is thanked for its help in the development of this work through the ARCHI-CM project supported by the “Ministère de l’Enseignement Supérieur de la Recherche et de l’Innovation”, the region “Hauts-de-France”, the ERDF program of the European Union and the Métropole Européenne de Lille. The present research work has also been carried out in the ELSAT 2020 project supported by the European Union with the European Regional Development Fund, the French State, and the Hauts-de-France Region Council.

References

[1] J.-W. Yeh, S.-K. Chen, S.-J. Lin, J.-Y. Gan, T.-S. Chin, T.-T. Shun, C.-H. Tsau, S.-Y. Chang, Nanostructured high-entropy alloys with multiple principal elements: novel alloy design concepts and outcomes, Adv. Eng. Mater. 6 (2004) 299–303, https://doi.org/10.1002/adem.200300567.

[2] B. Cantor, I.T.H. Chang, P. Knight, A.J.B. Vincent, Microstructural development in equiatomic multicomponent alloys, Mater. Sci. Eng. A 375–377 (2004) 213–218, https://doi.org/10.1016/j.msea.2003.10.257.

[3] J.-W. Yeh, Recent progress in high-entropy alloys, <icepaste/> 31 (2006) 633–648, https://doi.org/10.3166/acsm.31.633-648.

[4] Y. Zhang, T.T. Zuo, Z. Tang, M.C. Gao, K.A. Dahmen, P.K. Liaw, Z.P. Lu, Microstructures and properties of high-entropy alloys, Prog. Mater. Sci. 61 (2014) 1–93, https://doi.org/10.1016/j.pmatsci.2013.10.001.

[5] H. Diao, X. Xie, F. Sun, K.A. Dahmen, P.K. Liaw, Mechanical properties of high-entropy alloys, in: High-Entropy Alloys, Springer International Publishing, Cham, 2016, pp. 181–236, https://doi.org/10.1007/978-3-319-27013-5_6.

[6] A. Ayyagari, C. Barthelemy, B. Gwalani, R. Banerjee, T.W. Scharf, S. Mukherjee, Reciprocating sliding wear behavior of high entropy alloys in dry and marine environments, Mater. Chem. Phys. 210 (2018) 162–169, https://doi.org/10.1016/j.matchemphys.2017.07.031.

[7] G. Deng, A.K. Tieu, L. Su, P. Wang, L. Wang, X. Lan, S. Cui, H. Zhu, Investigation into reciprocating dry sliding friction and wear properties of bulk CoCrFeNiMo high entropy alloys fabricated by spark plasma sintering and subsequent cold rolling processes: role of mo element concentration, Wear 460–461 (2020), 203440, https://doi.org/10.1016/j.wear.2020.203440.

[8] G. Deng, A.K. Tieu, X. Lan, L. Su, L. Wang, Q. Zhu, H. Zhu, Effects of normal load and velocity on the dry sliding tribological behaviour of CoCrFeNiMo0.2 high entropy alloy, Tribol. Int. 144 (2020), 106116, https://doi.org/10.1016/j.triboint.2019.106116.

[9] W. Li, P. Liu, P.K. Liaw, in: Microstructures and properties of high-entropy alloy films and coatings: a review 6, 2018, pp. 199–229, https://doi.org/10.1080/21663831.2018.1434248.

[10] T.S. Srivatsan, M. Gupta, High Entropy Alloys: Innovations, Advances, and Applications, CRC Press, 2020.

[11] B.R. Braeckman, F. Boydens, H. Hidalgo, P. Dutheil, M. Jullien, A.L. Thomann, D. Depla, High entropy alloy thin films deposited by magnetron sputtering of powder targets, Thin Solid Films 580 (2015) 71–76, https://doi.org/10.1016/j.tsf.2015.02.070.

[12] X. Feng, G. Tang, M. Sun, X. Ma, L. Wang, K. Yukimura, Structure and properties of multi-targets magnetron sputtered ZrNbTaTiW multi-elements alloy thin films, Surf. Coat. Technol. 228 (2013), https://doi.org/10.1016/j.surfcoat.2012.05.038.

[13] Y. Zhou, P. Kelly, Q.B. Sun, The characteristics of the plasma in a powder sputtering rig, Thin Solid Films 516 (2008) 4030–4035, https://doi.org/10.1016/j.tsf.2007.10.105.

[14] X.H. Yan, J.S. Li, W.R. Zhang, Y. Zhang, A brief review of high-entropy films, Mater. Chem. Phys. 210 (2018) 12–19, https://doi.org/10.1016/j.matchemphys.2017.07.078.

[15] A. Leyland, A. Matthews, On the significance of the H/E ratio in wear control: a nanocomposite coating approach to optimised tribological behaviour, Wear 246 (2000) 1–11, https://doi.org/10.1016/S0043-1648(00)00488-9.

[16] X. Chen, Y. Du, Y.-W. Chung, Commentary on using H/E and H/E as proxies for fracture toughness of hard coatings, Thin Solid Films 688 (2019), 137265, https://doi.org/10.1016/j.tsf.2019.04.040.

[17] C. Sha, Z. Zhou, Z. Xie, P. Munroe, FeMnNiCoCr-based high entropy alloy coatings: effect of nitrogen additions on microstructural development, mechanical properties and tribological performance, Appl. Surf. Sci. 507 (2020), 145101, https://doi.org/10.1016/j.apsusc.2019.145101.

[18] C. Sha, Z. Zhou, Z. Xie, P. Munroe, High entropy alloy FeMnNiCoCr coatings: enhanced hardness and damage-tolerance through a dual-phase structure and nanotwins, Surf. Coat. Technol. 385 (2020), 125435, https://doi.org/10.1016/j.surfcoat.2020.125435.

[19] X.B. Feng, W. Fu, J.Y. Zhang, J.T. Zhao, J. Li, K. Wu, G. Liu, J. Sun, Effects of nanotwins on the mechanical properties of AlxCoCrFeNi high entropy alloy thin films, Scr. Mater. 139 (2017) 71–76, https://doi.org/10.1016/J.SCRIPTAMAT.2017.06.009.

[20] C. Dang, J.U. Surjadi, L. Gao, Y. Lu, Mechanical properties of nanostructured CoCrFeNiMn high-entropy alloy (HEA) coating, Frontiers in Materials. 5 (2018), https://doi.org/10.3389/fmats.2018.00041.

[21] Y.-C. Hsu, C.-L. Li, C.-H. Hsueh, Modifications of microstructures and mechanical properties of CoCrFeMnNi high entropy alloy films by adding ti element, Surf. Coat. Technol. 399 (2020), 126149, https://doi.org/10.1016/j.surfcoat.2020.126149.

[22] W. Liao, S. Lan, L. Gao, H. Zhang, S. Xu, J. Song, X. Wang, Y. Lu, Nanocrystalline high-entropy alloy (CoCrFeNiAl0.3) thin-film coating by magnetron sputtering, Thin Solid Films 638 (2017) 383–388, https://doi.org/10.1016/j.tsf.2017.08.006.

[23] L. Zendejas Medina, L. Riekehr, U. Jansson, Phase formation in magnetron sputtered CrMnFeCoNi high entropy alloy, Surf. Coat. Technol. 403 (2020), https://doi.org/10.1016/j.surfcoat.2020.126323.

[24] T. Stasiak, S.N. Kumaran, M. Touzin, F. Béclin, C. Cordier, Novel multicomponent powders from the AlCrFeMnMo family synthesized by mechanical alloying, Adv. Eng. Mater. 21 (2019) 1900808, https://doi.org/10.1002/adem.201900808.

[25] P. Sudharshan Phani, W.C. Oliver, A critical assessment of the effect of indentation spacing on the measurement of hardness and modulus using instrumented indentation testing, Mater. Des. 164 (2019), 107563, https://doi.org/10.1016/j.matdes.2018.107563.

[26] W.C. Oliver, G.M. Pharr, An improved technique for determining hardness and elastic modulus using load and displacement sensing indentation experiments, J. Mater. Res. 7 (1992) 1564–1583, https://doi.org/10.1557/JMR.1992.1564.

[27] I. Hutchings, P. Shipway, 5 - Sliding wear, in: I. Hutchings, P. Shipway (Eds.), Tribology (Second Edition), Second Edition, Butterworth-Heinemann, 2017, pp. 107–164, https://doi.org/10.1016/B978-0-08-100910-9.00005-2.

[28] V. Dolique, A.L. Thomann, P. Brault, Y. Tessier, P. Gillon, Thermal stability of AlCoCrCuFeNi high entropy alloy thin films studied by in-situ XRD analysis, Surf. Coat. Technol. 204 (2010) 1989–1992, https://doi.org/10.1016/J.SURFCOAT.2009.12.006.

[29] S. Varalakshmi, M. Kamaraj, B.S. Murty, Formation and stability of equiatomic and nonequiatomic nanocrystalline CuNiCoZnAlTi high-entropy alloys by mechanical alloying, Metall. Mater. Trans. A 41 (2010) 2703–2709, https://doi.org/10.1007/s11661-010-0344-x.

[30] J.F. Moulder, W.F. Stickle, W.M. Sobol, K.D. Bomben, Handbook of X-ray Photoelectron Spectroscopy, 1992.

[31] L.Zendejas Medina, M.V.Tavares da Costa, E.M. Paschalidou, G. Lindwall, L. Riekehr, M. Korvela, S. Fritze, S. Kolozsvári, E.K. Gamstedt, L. Nyholm, U. Jansson, Enhancing corrosion resistance, hardness, and crack resistance in magnetron sputtered high entropy CoCrFeMnNi coatings by adding carbon, Materials & Design 205 (2021), 109711, https://doi.org/10.1016/j.matdes.2021.109711.

[32] U. Jansson, E. Lewin, Sputter deposition of transition-metal carbide films — a critical review from a chemical perspective, Thin Solid Films 536 (2013) 1–24, https://doi.org/10.1016/j.tsf.2013.02.019.

[33] S. Fritze, M. Hans, L. Riekehr, B. Osinger, E. Lewin, J.M. Schneider, U. Jansson, Influence of carbon on microstructure and mechanical properties of magnetron sputtered TaW coatings, Mater. Des. 196 (2020), 109070, https://doi.org/10.1016/j.matdes.2020.109070.

[34] U. Jansson, E. Lewin, Carbon-containing multi-component thin films, Thin Solid Films 688 (2019), 137411, https://doi.org/10.1016/j.tsf.2019.137411.

[35] S.J. Bull, Failure modes in scratch adhesion testing, Surf. Coat. Technol. 50 (1991) 25–32, https://doi.org/10.1016/0257-8972(91)90188-3.

[36] J. Joseph, N. Haghdadi, K. Shamlaye, P. Hodgson, M. Barnett, D. Fabijanic, The sliding wear behaviour of CoCrFeMnNi and AlxCoCrFeNi high entropy alloys at elevated temperatures, Wear 428–429 (2019) 32–44, https://doi.org/10.1016/j.wear.2019.03.002.

[37] K. Hiratsuka, A. Enomoto, T. Sasada, Friction and wear of Al2O3, ZrO2 and SiO2 rubbed against pure metals, Wear 153 (1992) 361–373, https://doi.org/10.1016/0043-1648(92)90176-9.

[38] H. Czichos, T. Saito, L. Smith, Springer Handbook of Materials Measurement Methods, Springer Berlin Heidelberg, Berlin, Heidelberg, 2006, https://doi.org/10.1007/978-3-540-30300-8.

[39] J.-M. Wu, S.-J. Lin, J.-W. Yeh, S.-K. Chen, Y.-S. Huang, H.-C. Chen, Adhesive wear behavior of AlxCoCrCuFeNi high-entropy alloys as a function of aluminum content, Wear 261 (2006) 513–519, https://doi.org/10.1016/j.wear.2005.12.008.